Volume 5
Number 12
December 2025
Pages 1265–1356

Environmental Science
Atmospheres

rsc.li/esatmospheres

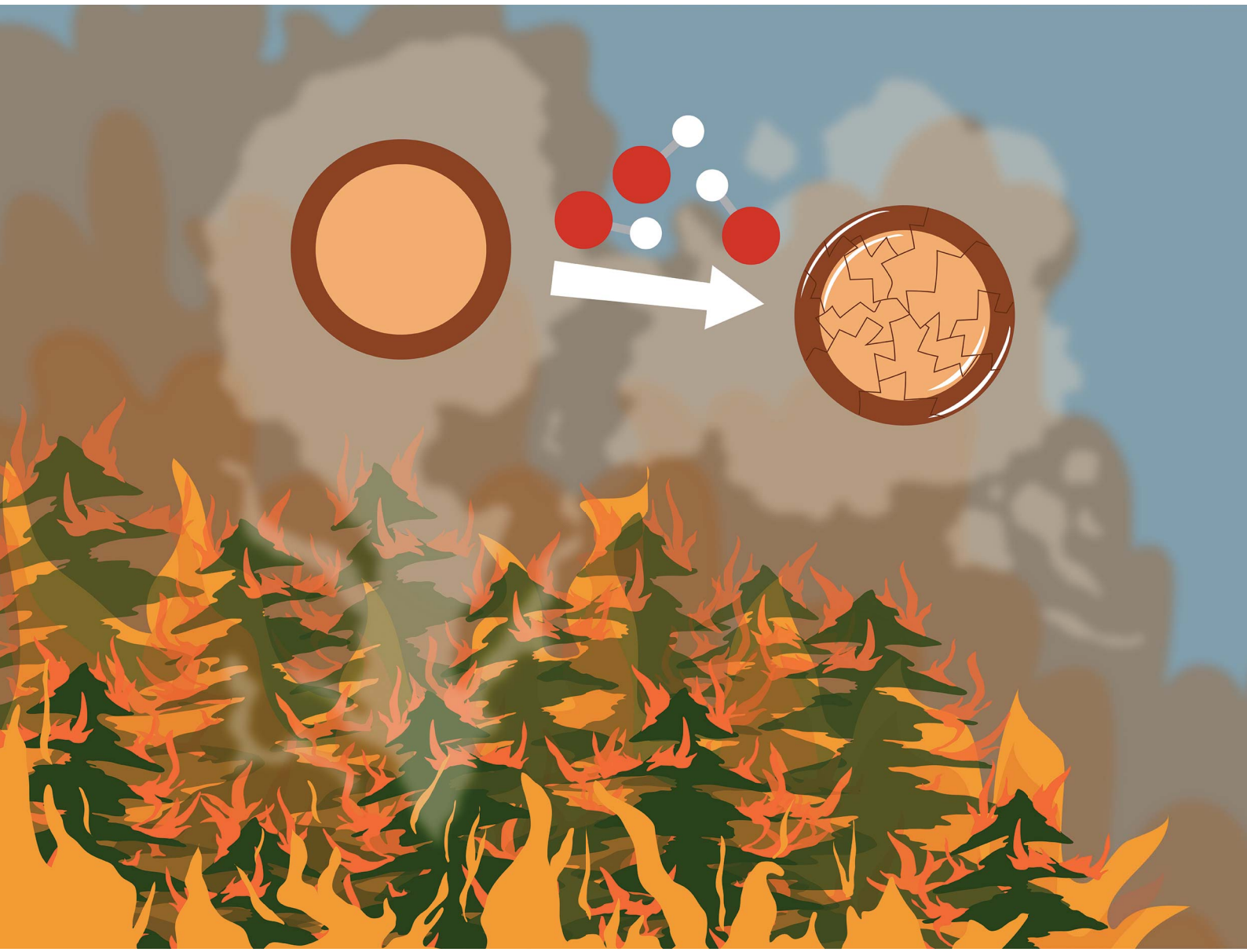

ISSN 2634-3606

ROYAL SOCIETY OF CHEMISTRY

PAPER
Allan K. Bertram *et al.*
Two-phase morphology and drastic viscosity changes in biomass burning organic aerosol after hydroxyl radical aging

Environmental Science: Atmospheres

ROYAL SOCIETY OF CHEMISTRY

PAPER

View Article Online
View Journal | View Issue

Cite this: *Environ. Sci.: Atmos.*, 2025, **5**, 1270

Two-phase morphology and drastic viscosity changes in biomass burning organic aerosol after hydroxyl radical aging

Nealan G. A. Gerrebos, Lyle P. F. Browning, Sepehr Nikkho, Evan R. Chartrand, Julia Zaks, Changda Wu and Allan K. Bertram *

Understanding the impact of wildfire-derived biomass burning organic aerosol (BBOA) on air quality, climate, and atmospheric chemistry requires knowledge of its phase behavior and viscosity – properties that remain poorly characterized after atmospheric aging. We investigated how hydroxyl radical (OH) aging affects these properties in BBOA generated from smoldering pine wood. Samples were aged in an oxidative flow reactor with equivalent atmospheric aging times of 1.3, 5.2, and 8.6 days. Phase behavior was assessed using optical microscopy, and viscosity was measured using the poke-flow technique. Across all aging times and relative humidities (0–90% RH), particles consisted of a hydrophilic core and a hydrophobic shell. Under dry conditions, viscosity increased by 4–5 orders of magnitude with aging, and the most aged particles became glass-like. Viscosity was strongly RH-dependent. From these measurements, we estimated mixing times and glass formation in 200 nm particles throughout the troposphere. Aged BBOA is predicted to remain well mixed in the boundary layer, but in the free troposphere (~1–12 km), mixing times often exceed 1 hour and particles are frequently in a glassy state. These findings have implications for particle growth, evaporation, and ice nucleation, and suggest that OH aging alone cannot fully explain tar ball formation in the atmosphere.

Received 22nd July 2025
Accepted 9th October 2025

DOI: 10.1039/d5ea00084j

rsc.li/esatmospheres

Environmental significance

Biomass burning organic aerosol (BBOA), a major category of emissions from wildfires, has large impacts on the climate and human health. To accurately predict these impacts, modelers need to understand BBOA's viscosity and the number of phases. These properties evolve over time as BBOA is "aged" by reactions with atmospheric oxidants such as OH radicals. We measured the viscosity of BBOA ranging from fresh to over a week old, and found the viscosity increased by 4–5 orders of magnitude, eventually becoming glass-like under dry conditions, and always contained two separate organic phases. Both of those findings are contrary to what most chemical transport models currently assume. This means that in the free troposphere, predictions of BBOA may be inaccurate.

Introduction

Aerosols are a significant component of the atmosphere and, without exception, are found throughout it.[1] Biomass burning is one of the major sources of organic aerosols to the atmosphere.[2–4] Biomass burning directly emits primary organic aerosol while also emitting volatile organic compounds (VOCs), which can be oxidized to become less volatile and condense into secondary organic aerosol (SOA).[5] The combination of primary organic aerosol and SOA from biomass burning is referred to as biomass burning organic aerosol (BBOA). The production of BBOA from wildfires is expected to rise as forest fires increase in frequency across the world.[6–9] This expected increase in BBOA emissions into the atmosphere increases the importance of understanding the behaviour of BBOA.

BBOA has broad impacts on human health, the climate, and stratospheric ozone,[10–21] and modeling and predicting BBOA's impact requires understanding its physical and chemical properties. Viscosity is one key property needed to understand the behaviour of BBOA. The viscosity of BBOA influences its reactivity by limiting the diffusion rates of reactants involved in heterogenous chemistry,[22–24] which affects the chemical composition of BBOA over its lifetime in the atmosphere and thus its hygroscopicity, light-absorbing properties, and toxicity.[25–29] High viscosity also slows the uptake and removal of semi-volatile organic compounds by BBOA particles, especially at colder and drier conditions, potentially affecting their growth and evaporation rates.[30] The number of phases present in an aerosol is another property that influences its behaviour and impacts. Understanding the number of phases is important

Department of Chemistry, University of British Columbia, Vancouver, British Columbia V6T 1Z1, Canada. E-mail: bertram@chem.ubc.ca

because it may affect processes such as chemical reactivity, optical properties, cloud nucleating ability, and the transport of gases or other particles within or through the aerosol.[31–34]

After being emitted into the atmosphere, all aerosols undergo "aging" – a set of chemical and physical changes driven by processes such as mixing, evaporation, condensation, exposure to sunlight, and reactions with atmospheric components, particularly oxidants.[35,36] The main atmospheric oxidants are ozone (O_3), hydroxyl radicals (OH), and nitrate radicals (NO_3). OH is the dominant oxidant during the day, NO_3 becomes important at night, and O_3 is active both day and night.[35] This study focuses specifically on aging caused by OH radicals.

Only a few studies have examined how OH aging affects the viscosity of biomass burning organic aerosol (BBOA). Kiland *et al.* investigated the viscosity of SOA formed by OH oxidation of biomass burning VOCs in an environmental chamber.[37] They showed that the resulting SOA exhibited viscosities higher than that of tar pitch at relative humidities (RH) below 10%. Xu *et al.* measured the volatility of BBOA produced from 12 different fuels before and after the equivalent of 1.5 days of atmospheric OH aging.[38] Based on these volatility measurements and changes in the oxygen-to-carbon ratio (O/C), they estimated particle viscosity before and after aging and found increases in viscosity for biomass burning combustion emissions. Because the study only examined up to 1.5 days of aging, the effect of longer-term OH aging remains unknown.

There has been little research into the number of phases within the organic portion of biomass burning emissions. Models simulating the microphysics, chemical evolution, concentration, or radiative properties of wildfire smoke typically assume that BBOA comprises only a single phase.[25,39–41] However, some recent studies have suggested otherwise. In transmission electron microscopy studies, Jahn *et al.* found BBOA particles with two separate organic phases in a core–shell morphology.[42] Gregson *et al.* showed that fresh pine BBOA comprises two separate organic phases, a polar core and a non-polar shell.[32] More recently, we found that field-sampled BBOA, collected 3 to 12 hours downwind of forest fires, also had two phases.[43] However, the precise age of the BBOA in that experiment could not be determined, and the number of organic phases present in BBOA after aging for a day or longer is unknown.

To assess the effects of different aging times on the viscosity and number of phases of BBOA, we generated BBOA from pine wood under smoldering conditions and then used an oxidative flow reactor (OFR) to age samples of BBOA for the equivalent of 1.3, 5.2, and 8.6 days of atmospheric aging. Following this, we measured the aged BBOA's phase behaviour with optical microscopy and its viscosity with the poke-flow technique.

Experimental

BBOA sample production

BBOA was generated by burning 0.4 g of pine wood in a custom tube furnace following the design of Kim *et al.* (Fig. S1).[44] The tube furnace consisted of a glass tube surrounded by a ceramic ring furnace that wraps around the tube. The pine wood was cut into 2 mm-by-2 mm pieces and laid along the glass tube so that there was a continuous line of fuel along the tube for 5 cm. Zero air (Purge Gas Generator, MTI Puregas) flowed at 3 L min^{-1} through the tube. The ceramic ring furnace was mounted to a custom track which moved along the length of the tube at a speed of 1 cm min^{-1} to ensure constant production of BBOA throughout the burning. The temperature of the furnace was 400 °C to simulate the smoldering conditions of a forest fire and produce minimal black carbon. During BBOA generation the output of the tube furnace was connected to a 200 L steel barrel. After all the wood had been burnt, the barrel was disconnected from the tube furnace and connected to a Potential Aerosol Mass oxidative flow reactor (PAM-OFR, Aerodyne Research Inc.). To ensure proper mixing and to prevent settling, a brushless fan (CG12038H12-IP67, Coolerguys) was placed at the bottom of the barrel facing upwards and turned on for the whole experiment. The barrel was electrically grounded to prevent enhanced deposition of charged BBOA particles on the walls of the barrel.

Oxidative flow reactor

Fig. S2 details the set-up of the oxidative flow reactor. BBOA samples were pulled from the barrel through the PAM-OFR using a downstream vacuum pump (Varian, SH-100). The amount of BBOA introduced was controlled by adjusting the vacuum pump and the zero air flowing into the OFR. Both sets of internal lamps (185 and 254 nm) were turned on and their voltages changed to adjust OH exposure. The RH in the OFR was roughly constant at 55–60%. The 185 and 254 nm lamps were always at the same voltage as each other (Table S1). After a particle residence time of 173 s in the chamber, the BBOA flowed through an ozone denuder and was sent to a multi-orifice single stage particle impactor (MOSSI, MSP Corporation), aerosol mass spectrometer (HR-ToF-AMS, Aerodyne Research Inc.), and scanning mobility particle sizer consisting of a Differential Mobility Analyzer (Model 3080, TSI Inc., sheath gas flow of 1.8 L min^{-1}) and an Ultrafine Condensation Particle counter (model 3776, TSI Inc.) (detection range: 20.2–947.5 nm diameter). In the impactor, BBOA particles were collected on 12 mm glass microscope cover slips (BoliOptics) with a hydrophobic coating (Flouropel-800, Cytonix). At the exit of the reactor, the following gases were measured: ozone (UV-100, Eco Sensors), CO (48i, Thermo Scientific) and SO_2 (43i-TLE, Thermo Scientific).

OH exposure, with units of concentration-time, is a measure of the concentration of oxidizing species and the length of time that samples are exposed to these species. OH exposure was determined by measuring the concentrations of gas tracers passing through the OFR and monitoring their decay at different UV lamp voltages. Pseudo first-order rate kinetics were then applied to the decays in gas tracer concentration to get the OH exposure (see SI Section S1 for full details). For gas tracers, we used CO generated from pine smoldering or pure SO_2 gas (Linde Canada Inc.) (SI Section S1, Fig. S3).

From the OH exposures, we calculated the equivalent atmospheric age using the following equation:

$$\text{Equivalent atmospheric age} = \frac{\text{OH exposure}}{\text{Average concentration of OH in the atmosphere}} \quad (1)$$

When calculating the equivalent atmospheric aging, we assumed an average tropospheric OH concentration of 1.5×10^6 molecules cm^{-3}.[45] Equivalent atmospheric ages used in our experiments, calculated with the CO gas tracer-derived OH exposures, were 0 days, 1.3 days, 5.2 days, and 8.6 days, which are atmospherically relevant based on an average 8 day lifetime of aerosols in the troposphere.[46] The OFR settings used in our experiments that gave these equivalent atmospheric ages are given in Table S1.

In the OFR, VOCs from the smoke were oxidized to form low volatility organic compounds (LVOCs). These LVOCs can: (a) condense on aerosol particles, (b) condense on the chamber walls, (c) exit the chamber in the gas phase and later condense on tubing walls due to the high surface to volume ratio, and (d) undergo further gas-phase reactions with OH, forming non-condensable products.[47,48] These fates should also apply to semivolatile organic compounds.[49]

To assess the fate of LVOCs, we applied the calculations described in Palm *et al.* (SI Section S2).[48] Based on these calculations, the dominant reaction pathway of the smoke under OH exposure in the PAM was LVOCs condensing on particles, contributing from 75% to 69% for equivalent atmospheric ages of 1.3 days to 8.6 days (Fig. S4). Condensation onto particles is the dominant fate of LVOCs in the atmosphere.[48]

Aerosol mass spectrometry

An aerosol mass spectrometer (HR-ToF-AMS, Aerodyne Research Inc.) was used to measure the mass spectra of BBOA after the OFR.[50–52] Spectra were collected with a time resolution of one minute. The vaporizer current was set to 1 A. High-resolution AMS data were processed using Squirrel v1.66 and PIKA 1.26 in the Igor Pro software environment (WaveMetrics). Elemental ratios were estimated using the Improved Ambient method using peaks up to m/z 240, which contained 99% of the mass of all fragments for all samples.[53] For each sample, we report the mean oxygen-to-carbon ratio (O : C), hydrogen-to-carbon ratio (H : C), and carbon oxidation state ($\overline{OS}_C \approx 2 \times O:C - H:C$)(Table S1).[54]

Phase behavior

Phase behaviour was determined using an optical microscope (Axiotech 100 HD, Zeiss) and camera (FMA050, Amscope) coupled to a humidity-controlled cell with RH values between 0% and 90%.[55] Pure air was humidified using a bubbler in a refrigerated bath (NESLAB RTE-140, Thermo Scientific) and passed through the cell held at 20 °C. RH was calculated from the cell temperature and dew point temperature.[56]

Viscosity measurement

Viscosity was measured with the poke-flow method.[57,58] The apparatus is depicted in Fig. S5. The RH was controlled by adjusting the flows of dry and humidified pure air while the cell temperature was measured with a thermocouple (HH200A, Omega) and the dewpoint of the air exiting the cell was measured with a chilled mirror hygrometer (D-2, General Eastern).

Following equilibration, a fine needle (0.25 mm diameter with a tip size <30 μm, 13561-10 Ted Pella) attached to a hydraulic micromanipulator (MO-202, Narishige) was lowered into the center of a selected particle to create a circular deformation. The needle was then quickly withdrawn as a camera (MA1000, Amscope) fitted to an inverted optical microscope (ME1400TC-INF, Zeiss) was used to record the droplet flowing and the hole closing as the particle returned to its original shape. The time taken for the area-equivalent diameter of the hole to close by $\frac{1}{2}$ was recorded as the experimental flow time, τ_{exp}.

To determine the viscosity, each BBOA particle deformed by the needle was modelled as a half torus geometry using COMSOL Multiphysics software. The modelled time for the hole to close by $\frac{1}{2}$ of its diameter is compared to the τ_{exp} for each BBOA particle; the simulated viscosity is then adjusted from the initial estimate until the modelled time matches τ_{exp} within 5%. The comparison between the modelled time and τ_{exp} was done twice per particle; once assuming that the surface tension and the slip length are both large, which produces an upper limit to the viscosity, and once assuming the opposite, thereby producing a lower limit to the viscosity (see Table S2 for the parameters used in the simulations). Two special cases arise in which either only an upper limit or only a lower limit can be estimated. If the hole fully closes faster than the camera can capture (2 frames per second), then the upper bound of the viscosity is assumed to be the maximum viscosity that would allow for the hole to fully close in 0.5 s. We assume that the initial hole was the same area as the tip of the needle, which can be seen when the needle is fully depressed into the particle and touching the glass slide. On the other hand, if no movement is observed in >12 hours then it is assumed that the BBOA flowed <0.5 μm (the resolution of the camera), and the minimum viscosity required for the material to flow only 0.5 μm is used as the lower bound of viscosity.[57] This no-movement case is typically accompanied by cracking or shattering of the particle upon being poked.

In all the experiments the BBOA contained two phases: a larger inner phase, surrounded by a thin outer phase (see Results and discussion: phase behaviour below). In the poke-flow experiments, the needle pierced only the center of the particles, creating a hole in the inner phase while leaving the outer phase undisturbed (Video S1). No movement was observed in the outer phase during or after the poke, suggesting that the measured τ_{exp} reflects the properties of the inner phase. Consequently, the viscosity obtained from simulations corresponds to the inner phase. To validate this, we measured the viscosity of the inner phase of unaged BBOA at 0% RH using Fluorescence Recovery After Photobleaching (FRAP), as detailed in SI S3. Unlike poke-flow, FRAP enables separate measurements of the viscosity of each phase. However, FRAP is limited to viscosities $\leq 10^4$ Pa s and is not suitable for aged samples with higher viscosities, which is why it was not the main method used throughout this paper.

The viscosities obtained from FRAP were within the uncertainty range of the poke-flow results (Fig. S6), confirming that the poke-flow measurements reflect the viscosity of the inner phase in core–shell BBOA particles. Additionally, after aging and under dry conditions, particles often developed visible

cracks when poked (as mentioned above and shown below). These cracks extended from the hole all the way to the outer edge of the particle, through both the inner and outer phase. For such cases, we calculated a lower bound on viscosity. Since it was clear that both phases cracked and did not flow, the lower-bound viscosity applies to both phases, unlike the results for particles that flowed which can only be interpreted as applying to the inner phase.

Prior to poking the particles, samples were conditioned to the surrounding RH for at least 2 hours to allow for water to diffuse in/out of the particles. For dry particles that cracked and did not flow after poking, longer conditioning could not make a difference because it would only lead to less water content in the BBOA, and therefore they would still crack. For particles that flowed after poking and viscosities of 10^7 Pa s or less, we carried out a separate set of experiments that showed that longer conditioning times did not change poke flow results, indicating that 2 hours is sufficient for these types of particles (SI Section S3 and Fig. S7).[25,59]

Results and discussion

Chemical composition of the BBOA

AMS mass spectra of unaged and aged BBOA are shown in Fig. S8. In all cases, the aerosol was composed of more than 99% organic material. From these spectra, the average $\overline{OS}_C$ and O/C were calculated (Fig. 1A). Both $\overline{OS}_C$ and O/C increased substantially between 0 and 1.3 days of aging. Between 1.3 and 5.2 days, the values continued to rise but at a slower rate. From 5.2 to 8.6 days, there was only a very slight increase. These results (when taken along with SI Section S2 showing that most LVOCs still condense at high aging times) indicate that most oxidation occurs within the first few days of aging.

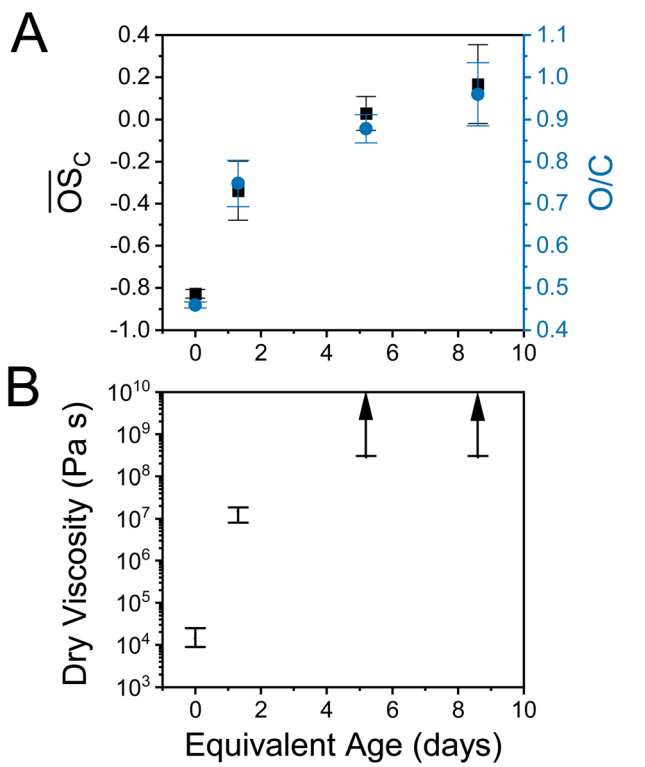

Fig. 1 (A) Carbon oxidation states and oxygen-to-carbon ratios as measured with an aerosol mass spectrometer, increasing with equivalent atmospheric age in the oxidative flow reactor. Error bars represent 1 standard deviation. (B) Increase in viscosity with equivalent atmospheric age. Error bars represent upper and lower limits of viscosity. Upwards arrows indicate that the upper limit could not be found and only lower limits are available.

Phase behavior

All samples showed two phases from 0% to 90% RH, regardless of the extent of aging (Fig. 2). For all particles, the morphology appeared as one core phase surrounded by a second outer phase, although the roundness of particles varied. The outer phase generally appeared to be thin and did not make up as much of the total BBOA as the inner phase did. The inner phase was identified as the hydrophilic/more polar phase because it grew when the RH was high, showing that it takes up more water from the atmosphere.

Previous studies suggest that phase separation in organic aerosols can be driven by polarity differences between phases, which are often approximated by differences in their O/C ratios. Large differences in O/C (≥0.47) are thought to promote phase separation.[60–62] Between the unaged and 8.6-day-aged samples, the average O/C of the whole particles increased from 0.46 to 0.96. However, the O/C values of the individual phases are unknown. With prolonged aging and oxidation, we expect the O/C of both phases to increase and eventually converge as the maximum oxygen content per carbon atom is approached. Surprisingly, such convergence apparently does not occur even after 8.6 days of aging, as the two phases remained distinct.

Although no studies have directly visualized the number of phases in BBOA after explicit OH aging, phase separation has been observed in both unaged and field-sampled BBOA. Previously, we studied unaged pine wood BBOA generated using the same method but with less dilution – likely representative of BBOA near its source – and observed two phases.[32] More recently, we examined extracts of field-sampled BBOA collected 3 to 12 hours downwind of forest fires and also observed two-phase BBOA.[43] Together, these studies indicate that BBOA can contain multiple phases, even after atmospheric aging.

BBOA in the atmosphere and in our OFR consists primarily of sub-micron particles, while the particles in Fig. 2 are super-micron droplets formed by many sub-micron particles being collected in the same area by the impactor. An important question that remains is whether the two phases observed in our experiments coexist in single sub-micron BBOA particles, or if they originate as separate particles that are only combined after colliding on the substrate in the impactor; that is, the degree of internal and external mixing of these two phases in our experiments is unknown. Some studies on field-sampled biomass burning particles have investigated the mixing state of individual sub-micron particles using scanning transmission X-ray microscopy with near-edge X-ray absorption fine structure spectroscopy (STXM-NEXAFS).[63–65] These studies conventionally focus on the broader classes of organic carbon, elemental

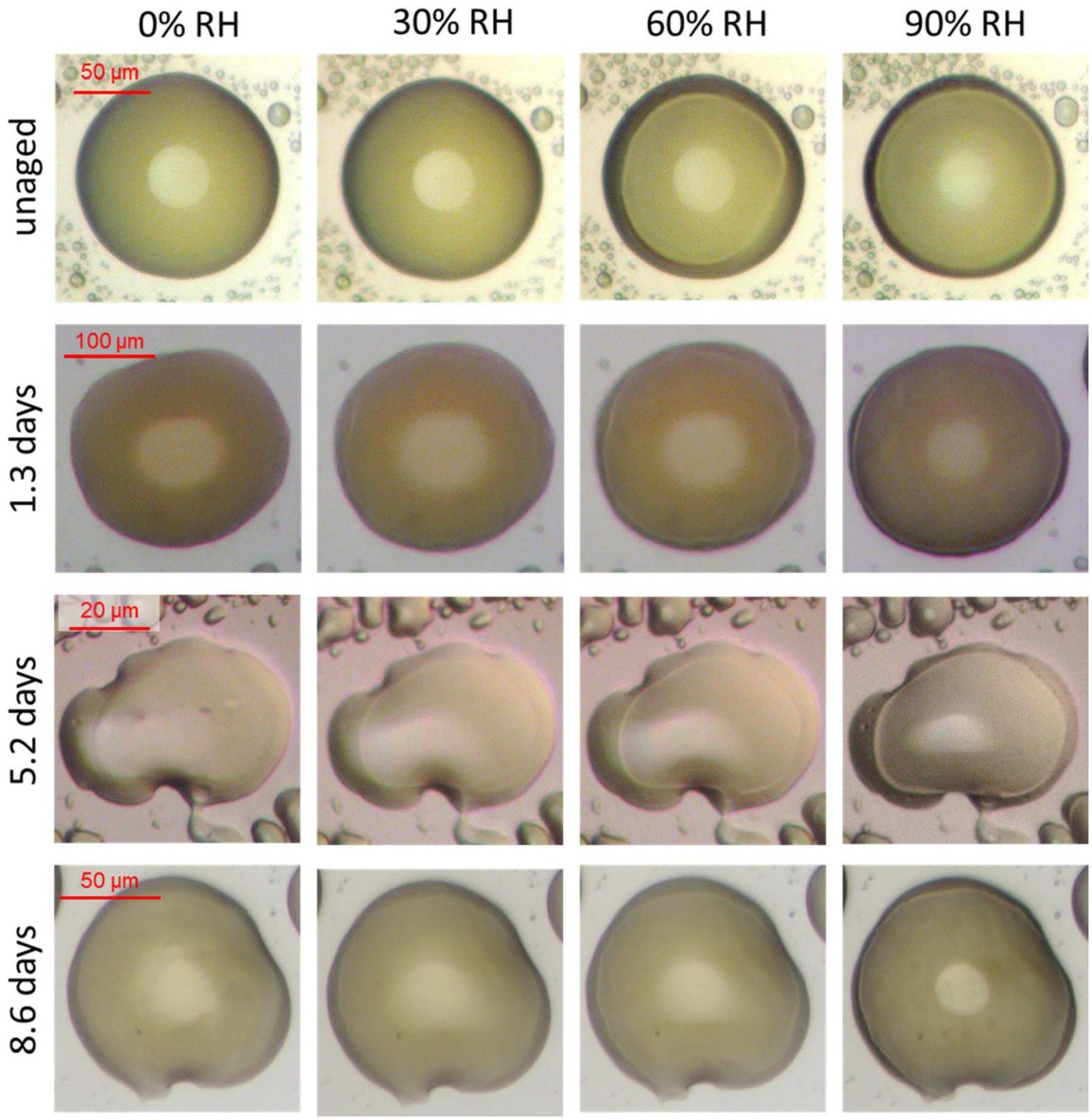

Fig. 2 Phase behaviour of unaged, 1.3, 5.2 and 8.6 days aged BBOA samples across a range of relative humidities (RH). Equivalent atmospheric ages are shown on the left and RH is shown along the top. White circles in the middle of most of the droplets are caused by reflections of the overhead microscope lamp, not separate phases.

carbon, and inorganic aerosols, whereas our analysis herein is focused on phase separation between two distinct types of organic carbon. However, if the two phases have different organic functionality, STXM-NEXAFS may be able to differentiate them. This should be explored in future studies.

Impacts of photochemical aging on viscosity

Examples of particle images before and after poking under dry conditions are shown in Fig. 3. For unaged samples, the recovery time after poking was approximately 10 seconds. In contrast, BBOA particles aged for 1.3 equivalent days took over 2.5 hours to recover. Particles aged for 5.2 and 8.6 days showed no observable recovery even after nearly 4 hours of monitoring. These aged samples also exhibited cracks and shard-like fragments after poking, indicating that the particles shattered like glass upon impact.

Viscosities were estimated from the recovery times after poking. Results for dry conditions are shown in Fig. 1B. For dry conditions, the viscosity of the unaged sample was 10^4 Pa s (comparable to peanut butter). After 1.3 days of aging, the viscosity increased to 10^7 Pa s, corresponding to a rise of 3 orders of magnitude. After 5 days, the viscosity was $\geq 3 \times 10^8$ Pa s (exceeding that of tar pitch) – a remarkable increase of at least 4 orders of magnitude compared to unaged BBOA. For longer aging times, any additional increase could not be detected, as the viscosity surpassed the upper limit measurable by the poke-flow technique.

The increase in viscosity with aging under dry conditions can be explained, at least in part, by the rise in $\overline{OS}_C$ and O/C of the

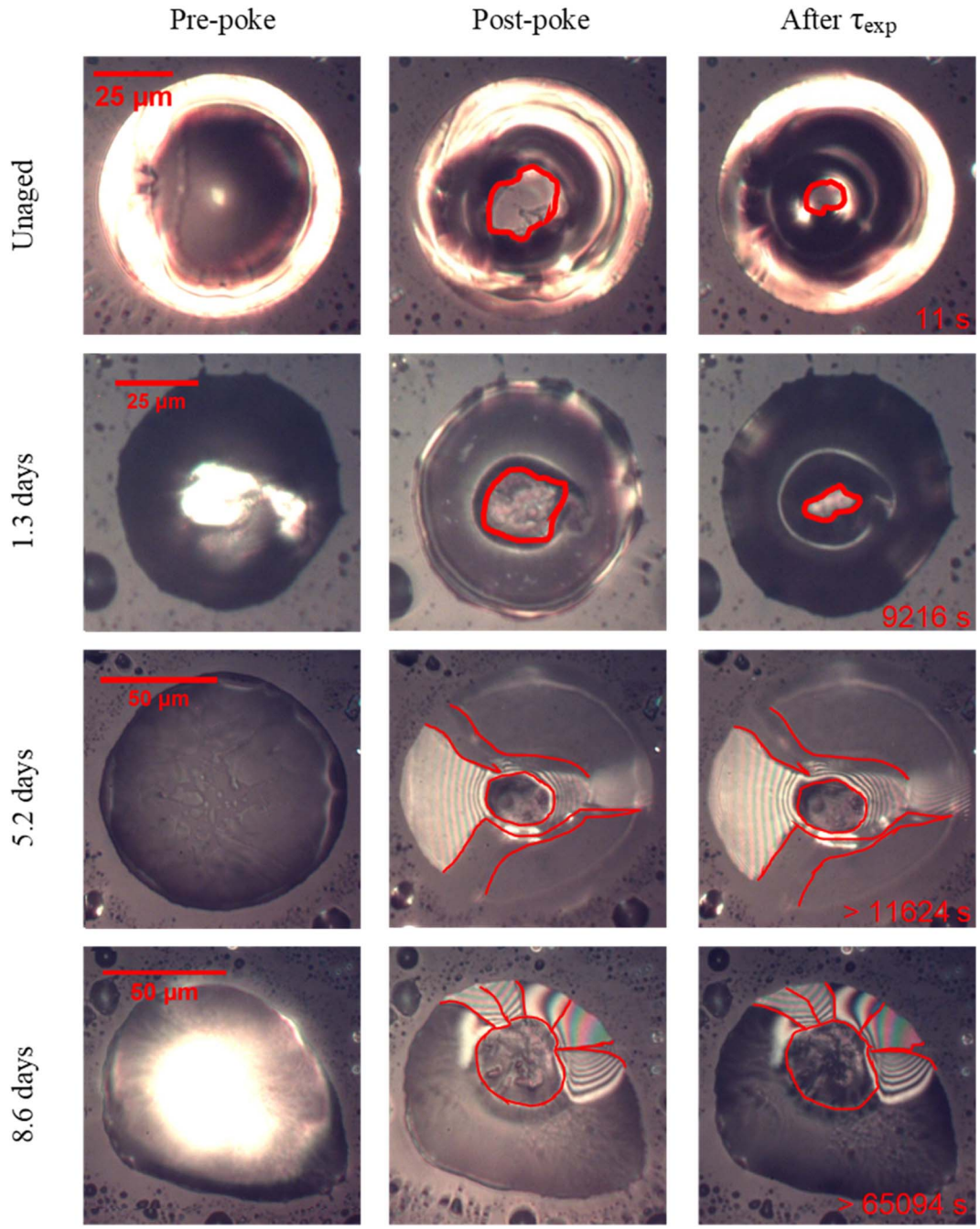

Fig. 3 Images taken of unaged, 1.3, 5.2 and 8.6-days aged particles before and after being poked at 0% RH. The top two rows show the recovery of the hole to $\frac{1}{4}$ of its initial area after 11 s (1st row) and 9216 s (2nd row). The bottom two rows show the particles cracking after being poked, indicating a potential glassy phase. The edges of the holes and cracks caused by the pokes are manually traced in red to increase visibility.

BBOA material over time (Fig. 1A). As $\overline{OS}_C$ and O/C increase, the polarity of the molecules in BBOA is expected to rise as well, leading to stronger intermolecular interactions and higher viscosity.[66–69] The leveling off in $\overline{OS}_C$ and O/C between 5 and 8 days of aging suggests that viscosity may also level off during this period. This interpretation is consistent with the lower-bound viscosity estimates for the 5.2- and 8.6-day aged samples (Fig. 1B).

Previous studies have used high resolution mass spectrometry to relate chemical composition in biogenic SOA to viscosity.[59,70,71] These methods are applicable to BBOA as well, and will be used in a future study to better elucidate the mechanisms responsible for aging.

Poke-flow experiments were conducted as a function of RH (Fig. 4). For all aging cases the viscosity of the inner phase strongly depended on RH. Take for example the results for 5.2 and 8.6 days of aging. Up to 10% RH, the inner phase viscosities were $\geq 10^8$ Pa s and the particles shattered. However, at approximately 50% RH the viscosities were $\leq 10^3$ Pa s – a decrease of at least 5 orders of magnitude with a 40% increase

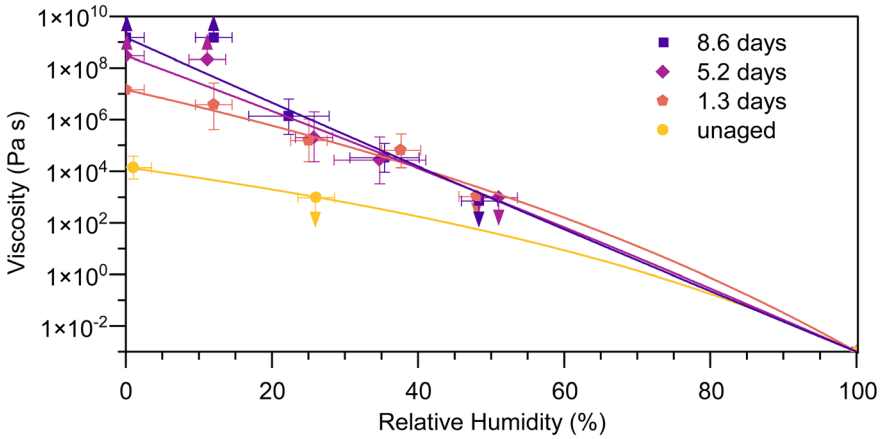

Fig. 4 Viscosities, measured by poke-flow, of unaged BBOA and BBOA aged for 1.3, 5.2 and 8.6 equivalent days. Upward pointing arrows show that points are only lower limits of viscosity, due to cracking and a glass-like behavior. Downward pointing arrows show that points are only upper limits of viscosity, due to the particles having such a low viscosity that closure of the poke hole was faster than the camera rate. Otherwise, plotted points are the median values between the upper and lower viscosity estimates returned by the model (shown as the y-error bars). X-error bars are due to the uncertainties in the hygrometers used for determining RH. Lines were determined by fitting a mass-based Arrhenius-type mixing equation for viscosity, using hygroscopicity as a fitting parameter and assuming the viscosity at 100% RH is equivalent to that of water (10^{-3} Pa s) (SI Section S5).

in RH. The slopes of the viscosity *versus* RH plots in Fig. 4 get steeper with higher aging times, which shows rising hygroscopicity as expected based on the rising $\overline{OS}_C$ and O/C (Fig. 1A). While the 1.3 day samples were less viscous than the 5.2 and 8.6 day samples under dry conditions, their viscosities are indistinguishable by 40% RH due to the more aged samples' higher hygroscopicities. The increase of BBOA viscosity due to OH-aging should be expected to be more impactful in dry parts of the atmosphere.

In Gregson *et al.*, we showed that the viscosity of the outer phase is different than that of the inner phase in unaged pine BBOA.[32] While the outer phase's viscosity can not be directly measured by poke-flow, it is clear that after 5.2 days and 8.6 days of equivalent aging the outer phase's viscosity has also increased to become $\geq 3 \times 10^8$ Pa s, because the cracks extend all the way to the outer edge of the particles (Fig. 3). Comparing to the outer phase viscosity measured in Gregson *et al.* (10^2–10^3 Pa s), this could represent a > 5 order of magnitude increase – although it

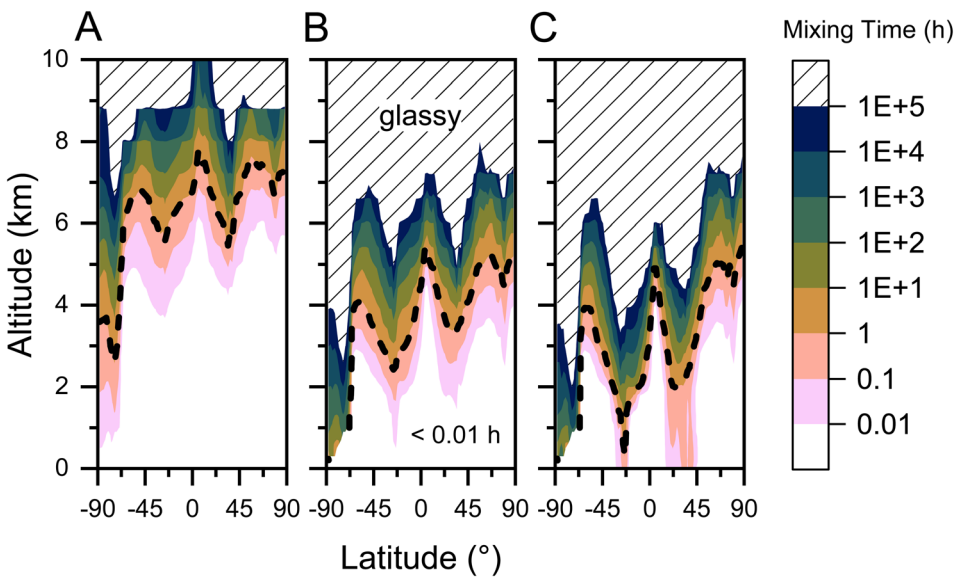

Fig. 5 Calculated mixing times as a function of altitude and latitude, based on average relative humidity and temperature from MERRA2 meteorological data, in a 200 nm diameter BBOA particle with (A) no aging, and (B) 1.3 days of equivalent atmospheric aging in the oxidative flow reactor and (C) 8.6 days of equivalent atmospheric aging in the oxidative flow reactor. Black dotted lines indicate 1 hour mixing times. The areas shaded with diagonal lines indicate conditions where the BBOA will be glassy, defined as >10^{12} Pa s, whereas blank white areas at the bottoms of the plots have mixing times of less than 0.01 h.

must be noted that the BBOA in Gregson *et al.* was less diluted before sampling so it should be expected to have a lower viscosity.

Kiland *et al.* oxidized phenolic VOCs (catechol, syringol and guaiacol), thought to be similar to those emitted from biomass burning, in a smog chamber with OH or O_3 as proxies for biomass burning SOA.[37,72] Viscosities of the resulting single-phased particles were measured with the poke flow method. Our aged BBOA viscosities, especially those of the 5.3 and 8.6 day old samples, closely match the viscosities of all four SOA proxies made by Kiland *et al.* (Fig. S9). This is consistent with the increased viscosity in our experiments being caused, at least partially, by the formation and mixing of secondary BBOA with the primary BBOA.

Similarly to our study, Xu *et al.* found that OFR aging of pine BBOA increases its viscosity.[38] Pine BBOA from flaming combustion was aged for approximately 1.5 equivalent atmospheric days in a PAM-OFR.[38] The viscosity of fresh and aged BBOA was estimated from volatility distributions and O/C measurements. For dry conditions, their predicted viscosities were 10^8 and 10^{10} Pa s for unaged and 1.3 day aged samples, respectively (Fig. S9) – a two order of magnitude increase. Notably, the calculated viscosities for their BBOA both before and after aging were higher than ours at comparable ages. A possible explanation for the difference in viscosity and behaviour is the differences in burning conditions, because we used lower smoldering temperatures while Xu *et al.* used flaming conditions. Furthermore, our study specifically measures the viscosity of the hydrophilic inner phase only, whereas volatility distribution calculations assume that the whole particle is one phase.

Conclusions and atmospheric implications

The presence of two phases in BBOA has important implications for predicting atmospheric processes relevant to air quality and climate. For example, a hydrophobic outer phase can enhance the ability of aerosols to nucleate liquid cloud droplets.[34,73] In another case, if the outer phase is more viscous than the inner phase, diffusion of species into the inner phase will be slower compared to a single-phase particle consisting of only the inner phase material.[32,74] Additionally, the equilibrium partitioning of semivolatile organic compounds depends on the number of phases: when only a single phase is present, the activity of semivolatile species within the condensed phase is lower, shifting equilibrium toward the condensed phase.[60,74,75] However, it is possible that BBOA is not internally mixed, and that the two phases we observed originated in two separate types of particle that each contain only one phase, only merging after sampling. In such a case, some of those effects (slow diffusion through the shell to reach the core) would not be observed. It is likely that atmospheric BBOA would have some mix of particles containing both phases and particles with just one of the two phases. Future studies should investigate the organic phase separation in sub-micron BBOA.

The viscosity of BBOA also has important implications for atmospheric processes. For example, viscosity influences both the heterogeneous chemistry and photochemistry of BBOA. High viscosity slows the diffusion of reactive gases into particles and the diffusion of unreacted condensed phase compounds to the particle surface, thereby limiting reaction rates.[76–79] It can also inhibit photodegradation by limiting the mobility of excited species within the particle.[80,81] In the case of BBOA, high viscosity can extend the atmospheric lifetime of brown carbon chromophores, allowing them to absorb sunlight and warm the atmosphere for longer periods.[25,32] Similarly, it can prolong the lifetime of carcinogenic polycyclic aromatic hydrocarbons, increasing the distance over which they can be transported.[23,82,83]

To further put the viscosity results into atmospheric context, we used our room temperature viscosity results as a function of RH to calculate viscosity and mixing times as a function of both RH and temperature following the procedure outlined in Maclean *et al.* and Schnitzler *et al.* (SI Section S5).[25,84] We then combined this information with average RH and temperature values in the atmosphere to calculate mixing times of organic molecules within 200 nm BBOA particles as a function of latitude and altitude (Fig. 5). The latitudes and altitudes at which the BBOA particles were in a glassy state (viscosity > 10^{12} Pa s) were also identified from these calculations. Chemical transport models often assume that organic aerosols are well mixed and in equilibrium with the gas phase on timescales shorter than the model time step, which is typically 0.5 to 1 hour in global models.[41,85–88] For unaged BBOA, this assumption is valid for most latitudes below 6 km, where mixing times are less than one hour (Fig. 5A). After 1.5 and 8.6 days of aging, the well-mixed assumption holds for most latitudes below approximately 3 km and 2 km, respectively (Fig. 5B and C).

These results suggest that BBOA, if similar to the material studied here, will remain well mixed in the planetary boundary layer (up to roughly 1 km), even after extended aging. However, the assumption of well mixed aerosol may not hold in much of the free troposphere (roughly 1–12 km), particularly for aged BBOA. Since BBOA plumes can rise above the boundary layer and enter the free troposphere, the longer mixing times at higher altitudes are relevant.[89–91] Incorporating these effects into chemical transport models may be important, as long mixing times can limit the evaporation and condensation of semivolatile organic compounds, thereby affecting SOA formation and loss.[92,93]

Glassy BBOA could also act as an ice nucleating substance in the atmosphere, modifying the frequency and properties of ice containing clouds.[94–100] Freshly emitted BBOA is predicted to only be glassy in the highest parts of the troposphere, mainly above 8 km in altitude (Fig. 5A). After 1 day of aging, however, glassy BBOA is likely to occur as low as 5 or 6 km (Fig. 5B). After 8.6 days of aging, BBOA should be glassy above an altitude of only 4 km in many parts of the troposphere, and 3 km close to the South Pole (Fig. 5C). The RH and temperature fields used for Fig. 5 are averaged across seasons and longitude, so there are likely times of year and regions where glassy BBOA occurs even lower. Studies are needed on the ice nucleation ability of glassy BBOA, since not all studies agree on the importance of glassy organic aerosols to atmospheric ice formation.[101]

Tar balls are a well-documented class of particles associated with biomass burning.[102–105] They are highly viscous, carbonaceous particles that retain a spherical shape after collection and remain stable under electron beam analysis in a vacuum. Their viscosity is estimated to exceed 10^9 Pa s, based on their "no flow" behavior and the fact that they do not coalesce upon coagulation.[106] Observations indicate that tar balls do not take up water until RH exceeds 75% RH,[107] and often much higher.[108,109] Electron microscope images of tar balls collected from the atmosphere suggest they can form through aging of BBOA, within ~3 hours.[104,105,110,111] Aging by OH radicals is a possible formation mechanism.[102] However, while our ≥ 5.3-day aged BBOA samples exhibited viscosities similar to tar balls under dry conditions, their viscosities at 50% RH were much lower (<10^3 Pa s), indicating hygroscopicity that is inconsistent with tar balls. Our results suggest that OH aging, under conditions similar to those used in this study and for the types of particles examined, cannot fully explain tar ball formation. Alternative mechanisms include evaporation of volatile BBOA components during dilution, nighttime aging by NO_3 radicals, or UV aging.[71,112–115]

Author contributions

Conceptualization: NGAG, LPFB, SN, AKB. Formal analysis: NGAG, LPFB, SN, ERC, JZ. Funding acquisition: AKB. Investigation: NGAG, LPFB, SN, ERC, JZ, CW. Methodology: NGAG, LPFB, SN, AKB. Project administration: AKB. Resources: AKB. Supervision: AKB. Validation: NGAG, LPFB, SN, ERC, CW. Visualization: NGAG, LPFB, ERC, JZ. Writing – original draft: LPFB. Writing – review and editing: NGAG, LPFB, ERC, JZ, CW, AKB.

Conflicts of interest

There are no conflicts to declare.

Data availability

AMS spectra, PAM-OFR calibration data, BBOA sampling logs, LVOC fate calculations, and all the data for all the figures are available at: **https://osf.io/q2rke/?view_only=86cd1282efc24373b7bf0380368d056c**.

Supplementary information: explanations of experiment validations (Section S1 to S4); calculations of mixing times (Section S5); additional figures and tables including experiment setup/apparatus, mass spectra, comparison to other studies (Tables S1, S2 and Fig. S1–S12) (DOCX). Video showing a poke flow experiment (Video S1) (AVI). See DOI: **https://doi.org/10.1039/d5ea00084j**.

Acknowledgements

We acknowledge the support of the Natural Sciences and Engineering Research Council of Canada (NSERC), [funding reference number RGPIN-2023-05333]. Cette recherche a été financée par le Conseil de recherches en sciences naturelles et en génie du Canada (CRSNG), [numéro de référence RGPIN-2023-05333]. We also acknowledge the support of NSERC for a postgraduate scholarship award [PGS D-579464-2023] for funding N. G. A. G. The Scientific colour map batlow is used in Fig. 5 to prevent visual distortion of the data and exclusion of readers with colour-vision deficiencies (**https://www.fabiocrameri.ch/colourmaps/**).

References

1 J. H. Seinfeld, in *Encyclopedia of Atmospheric Sciences*, ed. J. R. Holton, Academic Press, Oxford, 2003, pp. 2349–2354.
2 A. P. Tsimpidi, V. A. Karydis, S. N. Pandis and J. Lelieveld, *Atmos. Chem. Phys.*, 2016, **16**, 8939–8962.
3 M. O. Andreae, *Atmos. Chem. Phys.*, 2019, **19**, 8523–8546.
4 T. C. Bond, S. J. Doherty, D. W. Fahey, P. M. Forster, T. Berntsen, B. J. Deangelo, M. G. Flanner, S. Ghan, B. Kärcher, D. Koch, S. Kinne, Y. Kondo, P. K. Quinn, M. C. Sarofim, M. G. Schultz, M. Schulz, C. Venkataraman, H. Zhang, S. Zhang, N. Bellouin, S. K. Guttikunda, P. K. Hopke, M. Z. Jacobson, J. W. Kaiser, Z. Klimont, U. Lohmann, J. P. Schwarz, D. Shindell, T. Storelvmo, S. G. Warren and C. S. Zender, *J. Geophys. Res.:Atmos.*, 2013, **118**, 5380–5552.
5 J. Chen, C. Li, Z. Ristovski, A. Milic, Y. Gu, M. S. Islam, S. Wang, J. Hao, H. Zhang, C. He, H. Guo, H. Fu, B. Miljevic, L. Morawska, P. Thai, Y. F. Lam, G. Pereira, A. Ding, X. Huang and U. C. Dumka, *Sci. Total Environ.*, 2017, **579**, 1000–1034.
6 J. G. Canadell, C. P. (Mick) Meyer, G. D. Cook, A. Dowdy, P. R. Briggs, J. Knauer, A. Pepler and V. Haverd, *Nat. Commun.*, 2021, **12**, 6921.
7 M. Senande-Rivera, D. Insua-Costa and G. Miguez-Macho, *Nat. Commun.*, 2022, **13**, 1208.
8 J. T. Abatzoglou, D. S. Battisti, A. P. Williams, W. D. Hansen, B. J. Harvey and C. A. Kolden, *Commun. Earth Environ.*, 2021, **2**, 1–8.
9 K. Jiang, R. Xing, Z. Luo, W. Huang, F. Yi, Y. Men, N. Zhao, Z. Chang, J. Zhao, B. Pan and G. Shen, *Particuology*, 2024, **85**, 296–309.
10 K. Ballesteros-González, A. P. Sullivan and R. Morales-Betancourt, *Sci. Total Environ.*, 2020, **739**, 139755.
11 P. Bernath, C. Boone and J. Crouse, *Science*, 2022, **375**, 1292–1295.
12 S. Solomon, K. Stone, P. Yu, D. M. Murphy, D. Kinnison, A. R. Ravishankara and P. Wang, *Nature*, 2023, **615**, 259–264.
13 Y. Kuang, W. Xu, J. Tao, B. Luo, L. Liu, H. Xu, W. Xu, B. Xue, M. Zhai, P. Liu and Y. Sun, *Geophys. Res. Lett.*, 2024, **51**, e2023GL107147.
14 L. G. Jahl, T. A. Brubaker, M. J. Polen, L. G. Jahn, K. P. Cain, B. B. Bowers, W. D. Fahy, S. Graves and R. C. Sullivan, *Sci. Adv.*, 2021, **7**, eabd3440.
15 L. T. Fleming, P. Lin, J. M. Roberts, V. Selimovic, R. Yokelson, J. Laskin, A. Laskin and S. A. Nizkorodov, *Atmos. Chem. Phys.*, 2020, **20**, 1105–1129.
16 R. Saleh, *Curr. Pollut. Rep.*, 2020, **6**, 90–104.

17 C. E. Chung, V. Ramanathan and D. Decremer, *Proc. Natl. Acad. Sci. U. S. A.*, 2012, **109**, 11624–11629.
18 H. Brown, X. Liu, R. Pokhrel, S. Murphy, Z. Lu, R. Saleh, T. Mielonen, H. Kokkola, T. Bergman, G. Myhre, R. B. Skeie, D. Watson-Paris, P. Stier, B. Johnson, N. Bellouin, M. Schulz, V. Vakkari, J. P. Beukes, P. G. van Zyl, S. Liu and D. Chand, *Nat. Commun.*, 2021, **12**, 277.
19 N. H. F. French and A. T. Hudak, in *Landscape Fire, Smoke, and Health*, American Geophysical Union (AGU), 2023, pp. 69–88.
20 C. N. Vasilakopoulou, A. Matrali, K. Skyllakou, M. Georgopoulou, A. Aktypis, K. Florou, C. Kaltsonoudis, E. Siouti, E. Kostenidou, A. Błaziak, A. Nenes, S. Papagiannis, K. Eleftheriadis, D. Patoulias, I. Kioutsioukis and S. N. Pandis, *npj Clim. Atmos. Sci.*, 2023, **6**, 1–9.
21 K. Atwi, S. N. Wilson, A. Mondal, R. C. Edenfield, K. M. Symosko Crow, O. El Hajj, C. Perrie, C. K. Glenn, C. A. Easley, H. Handa and R. Saleh, *Atmos. Environ.*, 2022, **271**, 118929.
22 J. H. Kroll, C. Y. Lim, S. H. Kessler and K. R. Wilson, *J. Phys. Chem. A*, 2015, **119**, 10767–10783.
23 S. Zhou, M. Shiraiwa, R. D. McWhinney, U. Pöschl and J. P. D. Abbatt, *Faraday Discuss.*, 2013, **165**, 391–406.
24 T. Berkemeier, S. S. Steimer, U. K. Krieger, T. Peter, U. Poschl, M. Ammann and M. Shiraiwa, *Phys. Chem. Chem. Phys.*, 2016, **18**, 12662–12674.
25 E. G. Schnitzler, N. G. A. Gerrebos, T. S. Carter, Y. Huang, C. L. Heald, A. K. Bertram and J. P. D. Abbatt, *Proc. Natl. Acad. Sci. U. S. A.*, 2022, **119**(38), e2205610119.
26 M. Shiraiwa, M. Ammann, T. Koop and U. Pöschl, *Proc. Natl. Acad. Sci. U. S. A.*, 2011, **108**, 11003–11008.
27 F. H. Marshall, R. E. H. Miles, Y.-C. Song, P. B. Ohm, R. M. Power, J. P. Reid and C. S. Dutcher, *Chem. Sci.*, 2016, **7**, 1298–1308.
28 N. A. Hosny, C. Fitzgerald, A. Vyšniauskas, A. Athanasiadis, T. Berkemeier, N. Uygur, U. Pöschl, M. Shiraiwa, M. Kalberer, F. D. Pope and M. K. Kuimova, *Chem. Sci.*, 2016, **7**, 1357–1367.
29 Y. H. Kim, A. Sinha, I. J. George, D. M. DeMarini, A. P. Grieshop and M. I. Gilmour, *Sci. Total Environ.*, 2023, **892**, 164778.
30 M. Shiraiwa and J. H. Seinfeld, *Geophys. Res. Lett.*, 2012, **39**(24), DOI: **10.1029/2012GL054008**.
31 M. A. Freedman, *Chem. Soc. Rev.*, 2017, **46**, 7694–7705.
32 F. K. A. Gregson, N. G. A. Gerrebos, M. Schervish, S. Nikkho, E. G. Schnitzler, C. Schwartz, C. Carlsten, J. P. D. Abbatt, S. Kamal, M. Shiraiwa and A. K. Bertram, *Environ. Sci. Technol.*, 2023, **57**, 14548–14557.
33 A. Zuend and J. H. Seinfeld, *Atmos. Chem. Phys.*, 2012, **12**, 3857–3882.
34 P. Liu, M. Song, T. Zhao, S. S. Gunthe, S. Ham, Y. He, Y. M. Qin, Z. Gong, J. C. Amorim, A. K. Bertram and S. T. Martin, *Nat. Commun.*, 2018, **9**, 4076.
35 R. F. Hems, E. G. Schnitzler, C. Liu-Kang, C. D. Cappa and J. P. D. Abbatt, *ACS Earth Space Chem.*, 2021, **5**, 722–748.
36 N. M. Donahue, A. L. Robinson, E. R. Trump, I. Riipinen and J. H. Kroll, in *Atmospheric and Aerosol Chemistry*, ed V. F. McNeill and P. A. Ariya, Springer, Berlin, Heidelberg, 2014, pp. 97–143.
37 K. J. Kiland, F. Mahrt, L. Peng, S. Nikkho, J. Zaks, G. V. Crescenzo and A. K. Bertram, *ACS Earth Space Chem.*, 2023, **7**, 1388–1400.
38 W. Xu, Z. Li, Z. Zhang, J. Li, E. Karnezi, A. T. Lambe, W. Zhou, J. Sun, A. Du, Y. Li and Y. Sun, *J. Geophys. Res.:Atmos.*, 2023, **128**, e2022JD037911.
39 T. B. Zhuravleva, I. M. Nasrtdinov, I. B. Konovalov, N. A. Golovushkin and M. Beekmann, *Atmosphere*, 2021, **12**, 1555.
40 A. Akherati, Y. He, L. A. Garofalo, A. L. Hodshire, D. K. Farmer, S. M. Kreidenweis, W. Permar, L. Hu, E. V. Fischer, C. N. Jen, A. H. Goldstein, E. J. T. Levin, P. J. DeMott, T. L. Campos, F. Flocke, J. M. Reeves, D. W. Toohey, J. R. Pierce and S. H. Jathar, *Environ. Sci.: Atmos.*, 2022, **2**, 1000–1022.
41 D. Patoulias, E. Kallitsis, L. Posner and S. N. Pandis, *Atmosphere*, 2021, **12**, 1638.
42 L. G. Jahn, L. G. Jahl, B. B. Bowers and R. C. Sullivan, *ACS Earth Space Chem.*, 2021, **5**, 2184–2195.
43 N. G. A. Gerrebos, J. Zaks, F. K. A. Gregson, M. Walton-Raaby, H. Meeres, I. Zigg, W. F. Zandberg and A. K. Bertram, *Environ. Sci. Technol.*, 2024, **58**, 21716–21728.
44 Y. H. Kim, S. H. Warren, Q. T. Krantz, C. King, R. Jaskot, W. T. Preston, B. J. George, M. D. Hays, M. S. Landis, M. Higuchi, D. M. DeMarini and M. I. Gilmour, *Environ. Health Perspect.*, 2018, **126**, 017011.
45 J. Mao, X. Ren, W. H. Brune, J. R. Olson, J. H. Crawford, A. Fried, L. G. Huey, R. C. Cohen, B. Heikes, H. B. Singh, D. R. Blake, G. W. Sachse, G. S. Diskin, S. R. Hall and R. E. Shetter, *Atmos. Chem. Phys.*, 2009, **9**, 163–173.
46 C. Papastefanou, *Appl. Radiat. Isot.*, 2006, **64**, 93–100.
47 A. M. Ortega, P. L. Hayes, Z. Peng, B. B. Palm, W. Hu, D. A. Day, R. Li, M. J. Cubison, W. H. Brune, M. Graus, C. Warneke, J. B. Gilman, W. C. Kuster, J. de Gouw, C. Gutiérrez-Montes and J. L. Jimenez, *Atmos. Chem. Phys.*, 2016, **16**, 7411–7433.
48 B. B. Palm, P. Campuzano-Jost, A. M. Ortega, D. A. Day, L. Kaser, W. Jud, T. Karl, A. Hansel, J. F. Hunter, E. S. Cross, J. H. Kroll, Z. Peng, W. H. Brune and J. L. Jimenez, *Atmos. Chem. Phys.*, 2016, **16**, 2943–2970.
49 C. Bhattarai, V. Samburova, D. Sengupta, M. Iaukea-Lum, A. C. Watts, H. Moosmüller and A. Y. Khlystov, *Aerosol Sci. Technol.*, 2018, **52**, 1266–1282.
50 P. F. DeCarlo, J. R. Kimmel, A. Trimborn, M. J. Northway, J. T. Jayne, A. C. Aiken, M. Gonin, K. Fuhrer, T. Horvath, K. S. Docherty, D. R. Worsnop and J. L. Jimenez, *Anal. Chem.*, 2006, **78**, 8281–8289.
51 A. C. Aiken, P. F. Decarlo, J. H. Kroll, D. R. Worsnop, J. A. Huffman, K. S. Docherty, I. M. Ulbrich, C. Mohr, J. R. Kimmel, D. Sueper, Y. Sun, Q. Zhang, A. Trimborn, M. Northway, P. J. Ziemann, M. R. Canagaratna, T. B. Onasch, M. R. Alfarra, A. S. H. Prevot, J. Dommen,

J. Duplissy, A. Metzger, U. Baltensperger and J. L. Jimenez, *Environ. Sci. Technol.*, 2008, **42**, 4478–4485.
52 A. C. Aiken, P. F. DeCarlo and J. L. Jimenez, *Anal. Chem.*, 2007, **79**, 8350–8358.
53 M. R. Canagaratna, J. L. Jimenez, J. H. Kroll, Q. Chen, S. H. Kessler, P. Massoli, L. Hildebrandt Ruiz, E. Fortner, L. R. Williams, K. R. Wilson, J. D. Surratt, N. M. Donahue, J. T. Jayne and D. R. Worsnop, *Atmos. Chem. Phys.*, 2015, **15**, 253–272.
54 J. H. Kroll, N. M. Donahue, J. L. Jimenez, S. H. Kessler, M. R. Canagaratna, K. R. Wilson, K. E. Altieri, L. R. Mazzoleni, A. S. Wozniak, H. Bluhm, E. R. Mysak, J. D. Smith, C. E. Kolb and D. R. Worsnop, *Nat. Chem.*, 2011, **3**, 133–139.
55 M. T. Parsons, J. Mak, S. R. Lipetz and A. K. Bertram, *J. Geophys. Res.:Atmos.*, 2004, **109**(D6), DOI: 10.1029/2003JD004075.
56 O. A. Alduchov and R. E. Eskridge, *J. Appl. Meteorol. Climatol.*, 1996, **35**(4), 601–609.
57 J. W. Grayson, M. Song, M. Sellier and A. K. Bertram, *Atmos. Meas. Tech.*, 2015, **8**, 2463–2472.
58 L. Renbaum-Wolff, J. W. Grayson and A. K. Bertram, *Atmos. Chem. Phys.*, 2013, **13**, 791–802.
59 A. M. Maclean, N. R. Smith, Y. Li, Y. Huang, A. P. S. Hettiyadura, G. V. Crescenzo, M. Shiraiwa, A. Laskin, S. A. Nizkorodov and A. K. Bertram, *ACS Earth Space Chem.*, 2021, **5**, 305–318.
60 F. Mahrt, Y. Huang, J. Zaks, A. Devi, L. Peng, P. E. Ohno, Y. M. Qin, S. T. Martin, M. Ammann and A. K. Bertram, *Environ. Sci. Technol.*, 2022, **56**, 3960–3973.
61 F. Mahrt, L. Peng, J. Zaks, Y. Huang, P. E. Ohno, N. R. Smith, F. K. A. Gregson, Y. Qin, C. L. Faiola, S. T. Martin, S. A. Nizkorodov, M. Ammann and A. K. Bertram, *Atmos. Chem. Phys.*, 2022, **22**, 13783–13796.
62 F. Mahrt, E. Newman, Y. Huang, M. Ammann and A. K. Bertram, *Environ. Sci. Technol.*, 2021, **55**(18), 12202–12214.
63 G. W. Vandergrift, N. N. Lata, S. Mathai, A. Ijaz, Z. Cheng, M. Shrivastava, J. Zhang, A. S. M. Shawon, G. Kulkarni, L. R. Mazzoleni, W. Kew and S. China, *Environ. Sci.: Atmos.*, 2023, **3**, 1251–1261.
64 J. M. Tomlin, J. Weis, D. P. Veghte, S. China, M. Fraund, Q. He, N. Reicher, C. Li, K. A. Jankowski, F. A. Rivera-Adorno, A. C. Morales, Y. Rudich, R. C. Moffet, M. K. Gilles and A. Laskin, *Environ. Sci.: Atmos.*, 2022, **2**, 616–633.
65 F. A. Rivera-Adorno, J. M. Tomlin, N. N. Lata, L. Azzarello, M. A. Robinson, R. A. Washenfelder, A. Franchin, A. M. Middlebrook, S. China, S. S. Brown, C. J. Young, M. Fraund, R. C. Moffet and A. Laskin, *ACS EST Air*, 2025, **2**, 508–521.
66 N. E. Rothfuss and M. D. Petters, *Environ. Sci. Technol.*, 2017, **51**, 271–279.
67 N. E. Rothfuss and M. D. Petters, *Phys. Chem. Chem. Phys.*, 2017, **19**, 6532–6545.
68 J. W. Grayson, E. Evoy, M. Song, Y. Chu, A. Maclean, A. Nguyen, M. A. Upshur, M. Ebrahimi, C. K. Chan, F. M. Geiger, R. J. Thomson and A. K. Bertram, *Atmos. Chem. Phys.*, 2017, **17**, 8509–8524.
69 W.-S. W. DeRieux, Y. Li, P. Lin, J. Laskin, A. Laskin, A. K. Bertram, S. A. Nizkorodov and M. Shiraiwa, *Atmos. Chem. Phys.*, 2018, **18**, 6331–6351.
70 N. R. Smith, G. V. Crescenzo, Y. Huang, A. P. S. Hettiyadura, K. Siemens, Y. Li, C. L. Faiola, A. Laskin, M. Shiraiwa, A. K. Bertram and S. A. Nizkorodov, *Environ. Sci.: Atmos.*, 2021, **1**, 140–153.
71 V. J. Baboomian, G. V. Crescenzo, Y. Huang, F. Mahrt, M. Shiraiwa, A. K. Bertram and S. A. Nizkorodov, *Proc. Natl. Acad. Sci. U. S. A.*, 2022, **119**, e2208121119.
72 A. Akherati, Y. He, M. M. Coggon, A. R. Koss, A. L. Hodshire, K. Sekimoto, C. Warneke, J. de Gouw, L. Yee, J. H. Seinfeld, T. B. Onasch, S. C. Herndon, W. B. Knighton, C. D. Cappa, M. J. Kleeman, C. Y. Lim, J. H. Kroll, J. R. Pierce and S. H. Jathar, *Environ. Sci. Technol.*, 2020, **54**, 8568–8579.
73 M. B. Altaf, D. D. Dutcher, T. M. Raymond and M. A. Freedman, *ACS Earth Space Chem.*, 2018, **2**, 634–639.
74 M. Schervish and M. Shiraiwa, *Atmos. Chem. Phys.*, 2023, **23**, 221–233.
75 A. Zuend, C. Marcolli, T. Peter and J. H. Seinfeld, *Atmos. Chem. Phys.*, 2010, **10**, 7795–7820.
76 F. H. Marshall, T. Berkemeier, M. Shiraiwa, L. Nandy, P. B. Ohm, C. S. Dutcher and J. P. Reid, *Phys. Chem. Chem. Phys.*, 2018, **20**, 15560–15573.
77 J. H. Slade and D. A. Knopf, *Geophys. Res. Lett.*, 2014, **41**, 5297–5306.
78 Q. Z. Rasool, M. Shrivastava, Y. Liu, B. Gaudet and B. Zhao, *ACS Earth Space Chem.*, 2023, **7**, 1009–1024.
79 J. F. Davies and K. R. Wilson, *Chem. Sci.*, 2015, **6**, 7020–7027.
80 M. L. Hinks, M. V. Brady, H. Lignell, M. Song, J. W. Grayson, A. K. Bertram, P. Lin, A. Laskin, J. Laskin and S. A. Nizkorodov, *Phys. Chem. Chem. Phys.*, 2016, **18**, 8785–8793.
81 H. Lignell, M. L. Hinks and S. A. Nizkorodov, *Proc. Natl. Acad. Sci. U. S. A.*, 2014, **111**, 13780–13785.
82 S. Zhou, B. C. H. Hwang, P. S. J. Lakey, A. Zuend, J. P. D. Abbatt and M. Shiraiwa, *Proc. Natl. Acad. Sci. U. S. A.*, 2019, **116**, 11658–11663.
83 M. Shrivastava, S. Lou, A. Zelenyuk, R. C. Easter, R. A. Corley, B. D. Thrall, P. J. Rasch, J. D. Fast, S. L. Massey Simonich, H. Shen and S. Tao, *Proc. Natl. Acad. Sci. U. S. A.*, 2017, **114**, 1246–1251.
84 A. M. Maclean, Y. Li, G. V. Crescenzo, N. R. Smith, V. A. Karydis, A. P. Tsimpidi, C. L. Butenhoff, C. L. Faiola, J. Lelieveld, S. A. Nizkorodov, M. Shiraiwa and A. K. Bertram, *ACS Earth Space Chem.*, 2021, **5**, 3458–3473.
85 J. R. Odum, T. Hoffmann, F. Bowman, D. Collins, R. C. Flagan and J. H. Seinfeld, *Environ. Sci. Technol.*, 1996, **30**, 2580–2585.
86 G. N. Theodoritsi and S. N. Pandis, *Atmos. Chem. Phys.*, 2019, **19**, 5403–5415.
87 M. Hallquist, J. C. Wenger, U. Baltensperger, Y. Rudich, D. Simpson, M. Claeys, J. Dommen, N. M. Donahue, C. George, A. H. Goldstein, J. F. Hamilton, H. Herrmann, T. Hoffmann, Y. Iinuma, M. Jang, M. E. Jenkin,

J. L. Jimenez, A. Kiendler-Scharr, W. Maenhaut, G. McFiggans, T. F. Mentel, A. Monod, A. S. H. Prévôt, J. H. Seinfeld, J. D. Surratt, R. Szmigielski and J. Wildt, *Atmos. Chem. Phys.*, 2009, **9**, 5155–5236.

88 A. A. May, T. Lee, G. R. McMeeking, S. Akagi, A. P. Sullivan, S. Urbanski, R. J. Yokelson and S. M. Kreidenweis, *Atmos. Chem. Phys.*, 2015, **15**, 6323–6335.

89 R. Paugam, M. Wooster, S. Freitas and M. Val Martin, *Atmos. Chem. Phys.*, 2016, **16**, 907–925.

90 M. Val Martin, R. A. Kahn and M. G. Tosca, *Remote Sens.*, 2018, **10**, 1609.

91 B. Heinold, H. Baars, B. Barja, M. Christensen, A. Kubin, K. Ohneiser, K. Schepanski, N. Schutgens, F. Senf, R. Schrödner, D. Villanueva and I. Tegen, *Atmos. Chem. Phys.*, 2022, **22**, 9969–9985.

92 Y. Kim, K. Sartelet and F. Couvidat, *Atmos. Chem. Phys.*, 2019, **19**, 1241–1261.

93 R. A. Zaveri, J. E. Shilling, A. Zelenyuk, J. Liu, D. M. Bell, E. L. D'Ambro, C. J. Gaston, J. A. Thornton, A. Laskin, P. Lin, J. Wilson, R. C. Easter, J. Wang, A. K. Bertram, S. T. Martin, J. H. Seinfeld and D. R. Worsnop, *Environ. Sci. Technol.*, 2018, **52**, 1191–1199.

94 D. A. Knopf, P. A. Alpert and B. Wang, *ACS Earth Space Chem.*, 2018, **2**, 168–202.

95 M. J. Wolf, Y. Zhang, M. A. Zawadowicz, M. Goodell, K. Froyd, E. Freney, K. Sellegri, M. Rösch, T. Cui, M. Winter, L. Lacher, D. Axisa, P. J. DeMott, E. J. T. Levin, E. Gute, J. Abbatt, A. Koss, J. H. Kroll, J. D. Surratt and D. J. Cziczo, *Nat. Commun.*, 2020, **11**, 4834, DOI: **10.1038/s41467-020-18424-6**.

96 B. J. Murray, T. W. Wilson, S. Dobbie, Z. Cui, S. M. R. K. Al-Jumur, O. Möhler, M. Schnaiter, R. Wagner, S. Benz, M. Niemand, H. Saathoff, V. Ebert, S. Wagner and B. Kärcher, *Nat. Geosci.*, 2010, **3**, 233–237.

97 G. P. Schill and M. A. Tolbert, *Atmos. Chem. Phys.*, 2013, **13**, 4681–4695.

98 K. Ignatius, T. B. Kristensen, E. Järvinen, L. Nichman, C. Fuchs, H. Gordon, P. Herenz, C. R. Hoyle, J. Duplissy, S. Garimella, A. Dias, C. Frege, N. Höppel, J. Tröstl, R. Wagner, C. Yan, A. Amorim, U. Baltensperger, J. Curtius, N. M. Donahue, M. W. Gallagher, J. Kirkby, M. Kulmala, O. Möhler, H. Saathoff, M. Schnaiter, A. Tomé, A. Virtanen, D. Worsnop and F. Stratmann, *Atmos. Chem. Phys.*, 2016, **16**, 6495–6509.

99 A. D. James, J. S. A. Brooke, T. P. Mangan, T. F. Whale, J. M. C. Plane and B. J. Murray, *Atmos. Chem. Phys.*, 2018, **18**, 4519–4531.

100 M. F. Zeng, A. Zuend, N. G. A. Gerrebos, P. Yu, G. P. Schill, D. M. Murphy and A. K. Bertram, *ChemRxiv*, 2025, preprint, DOI: **10.26434/chemrxiv-2024-27934-v4**.

101 S. Kasparoglu, R. Perkins, P. J. Ziemann, P. J. DeMott, S. M. Kreidenweis, Z. Finewax, B. L. Deming, M. P. DeVault and M. D. Petters, *J. Geophys. Res.:Atmos.*, 2022, **127**, e2021JD036296.

102 M. Pósfai, A. Gelencsér, R. Simonics, K. Arató, J. Li, P. V. Hobbs and P. R. Buseck, *J. Geophys. Res.:Atmos.*, 2004, **109**(D6), D06213.

103 A. Tóth, A. Hoffer, I. Nyirő-Kósa, M. Pósfai and A. Gelencsér, *Atmos. Chem. Phys.*, 2014, **14**, 6669–6675.

104 K. Adachi, J. E. Dibb, J. M. Katich, J. P. Schwarz, H. Guo, P. Campuzano-Jost, J. L. Jimenez, J. Peischl, C. D. Holmes and J. Crawford, *EGUsphere*, 2024, 1–30.

105 M. Pósfai, R. Simonics, J. Li, P. V. Hobbs and P. R. Buseck, *J. Geophys. Res.:Atmos.*, 2003, **108**(D13), 8483.

106 J. P. Reid, A. K. Bertram, D. O. Topping, A. Laskin, S. T. Martin, M. D. Petters, F. D. Pope and G. Rovelli, *Nat. Commun.*, 2018, **9**, 956.

107 J. L. Hand, W. C. Malm, A. Laskin, D. Day, T. Lee, C. Wang, C. Carrico, J. Carrillo, J. P. Cowin, J. Collett Jr and M. J. Iedema, *J. Geophys. Res.:Atmos.*, 2005, **110**(D21), D21210.

108 K. Adachi and P. R. Buseck, *J. Geophys. Res.:Atmos.*, 2011, **116**(D5), D05204.

109 U. Dusek, G. P. Frank, G. Helas, Y. Iinuma, K. Zeromskiene, P. Gwaze, T. Hennig, A. Massling, O. Schmid, H. Herrmann, A. Wiedensohler and M. O. Andreae, *Geophys. Res. Lett.*, 2005, **32**(11), L11802.

110 K. Adachi, A. J. Sedlacek, L. Kleinman, S. R. Springston, J. Wang, D. Chand, J. M. Hubbe, J. E. Shilling, T. B. Onasch, T. Kinase, K. Sakata, Y. Takahashi and P. R. Buseck, *Proc. Natl. Acad. Sci. U. S. A.*, 2019, **116**, 19336–19341.

111 A. J. Sedlacek III, P. R. Buseck, K. Adachi, T. B. Onasch, S. R. Springston and L. Kleinman, *Atmos. Chem. Phys.*, 2018, **18**, 11289–11301.

112 H. H. Al-Mashala, K. L. Betz, C. T. Calvert, J. A. Barton, E. E. Bruce and E. G. Schnitzler, *ACS Earth Space Chem.*, 2023, **7**, 1882–1889.

113 H. H. Al-Mashala, M. Schervish, S. M. Liyanage, J. A. Barton, M. Shiraiwa and E. G. Schnitzler, *ACS EST Air*, 2025, **2**, 637–647.

114 Q. Xie, N. G. A. Gerrebos, D. Calderon-Arrieta, I. S. Morton, E. R. Halpern, C. Li, M. F. Zeng, A. K. Bertram, Y. Rudich and A. Laskin, *Environ. Sci. Technol.*, 2024, **58**, 18284–18294.

115 S. Nikkho, B. Bai, F. Mahrt, J. Zaks, L. Peng, K. J. Kiland, P. Liu and A. K. Bertram, *Environ. Sci. Technol.*, 2024, **58**, 21702–21715.